The Modified Envelope Orography and the Air Flow over and around Mountains

Li Long (李龙)
Beijing Meteorological Centre, State Meteorological Administration, Beijing 100081
and *Zhu Baozhen* (朱抱真)
Institute of Atmospheric Physics, Academia Sinica, Beijing, 100080
Received May 8, 1989

ABSTRACT

By use of the two-layer adiabatic globe spectral model and the zonally averaged climatic data of winter season as initial values, 10-day integrations are carried out based on three kinds of model topography (i.e., (1) the averaged topography; (2) the envelope topography; (3) the modified envelope topography). The results show that the orography of the Northern Hemisphere plays an important role in the simulation of large-scale weather patterns in winter season. The simulation based on the envelope topography developed by Wallace et al. has some improvements in the Rocky Mountains area. But this scheme causes very serious horizontal expansion around the Tibetan Plateau (hereafter referred to as the TP). A modified envelope topography scheme has been worked out that increases the slope of the TP by decreasing the horizontal expansion while keeping the maximum altitude. The results show some improvements of the scheme around the TP. By analysis of the mechanical effects of the large-scale orography on the currents, the different forcings of the air flow over and around the TP and the Rocky Mountain (the RM) are investigated.

I. INTRODUCTION

It is very crucial for the capability of numerical models to represent the impacts of orographys reasonably and accurately. The present works can be cataloged into two aspects:

(1) Due to the discretization of numerical models, errors are inevitable and will develop with the increase of the integration time. A lot of studies try to solve the problem, for example, the calculation of the pressure gradient force in the topography coordinate. In order to decrease the error caused by the discontinuity of orographys, some smooth processes are adopted. Despite of the advantage of the methods, sometimes the orographys are distorted severely.

(2) This kind of study pays more attentions to dynamic impacts of orography on air motions. For instance, the low-level blocking effect of obstacles is so seriously weakened by use of smooth orographys that the numerical results are poor. When simulating the Alps cyclogenesis, Dell'Osso, Radinovic (1984) used an artificially lifted orography while Egger (1972) explicitly enhanced the blocking effect by setting the low-level velocity to be zero in the region of orographys. Both of them obtained satisfactory results. Similar results were obtained by Mesinger and Strickler (1982) when they were simulating the Genoa cyclone. These results encourage more works on the processing of model topography.

When investigating the short-term system error of the ECMWF globe model, Wallace et al. (1983) found that the structure of the errors had some relation with the location of the Northern Hemisphere orographys (especially the Alps and the RM). Thus he introduced the

concept of so-called envelope topography, i.e., twice the standard deviation was added to the averaged topography. By utilizing the new topography scheme in the ECMWF operational forecast model, the total forecast scores have been raised. The main improvements are in the region of the RM. No obvious improvements appear in Asia. Through further study Jarrand *et al.* (1985) found that the effect of the envelope topography not only changed with seasons but also had relation with the resolution of the model. The improvements are chiefly obtained in the high-resolution spectral model. Further investigation of the effect of the envelope topography scheme in the low truncated spectral model needs to be improved.

When dealing with the cyclogenesis in the South China Sea during the winter monsoon, Tsai and Krishnamurti (1986) found some improvements by use of the envelope topography in East Asia, which was attributed to the steep slope of the new scheme used. This made the southward wind on the east side of the TP easier to reach the low latitudes. When investigating the mechanic impact of the orography on the formation of the southwest vortex, Wu and Chen (1984) showed that different model topographys (different altitudes, slopes and horizontal extension etc.) will cause different impacts.

The above mentioned averaged and envelope topography schemes can be regarded as different methods to deal with the sub-grid orography. As to its impacts on large-scale motions, there are still some other studies. For example, Egger (1970) parameterized a given isolate obstacle in the shallow water model. In early 60's, Eliassen and Palm (1961) carried out the creative work on the mechanism of upper propagated topographic steady waves. In recent years, based on this theory, Palmer (1987), Shutts (1985) *et al.* parameterized the topographic gravity waves forced by the sub-grid orographys and took into account the vertical propagation as well as the dissipation of the forced waves for large-scale motions. All these studies show the importance of the impacts of the sub-grid orographys on the large-scale motions.

By use of an adiabatic two-layer spectral model, effects of the averaged and envelope topography schemes in the model are investigated. And a modified envelope topography scheme is carried out. Possible reasons of the improvements are studied through the analysis of the mechanism of currents crossing and passing around the orography.

II. THE MODEL

The adiabatic two-layer spectral model is developed by Chen, Ji and Wu (1987). The scheme is obtained by revision of the adiabatic ECMWF spectral model into two layers.

(i) The governing equations are in σ-coordinates

$$\frac{\partial \xi}{\partial t} = \frac{1}{a(1-\mu^2)}\frac{\partial}{\partial \lambda}[F_v + P_v] - \frac{\partial}{a\partial \mu}[F_u + P_u], \tag{1}$$

$$\frac{\partial D}{\partial t} = \frac{1}{a(1-\mu^2)}\frac{\partial}{\partial \lambda}[F_u + P_u] + \frac{\partial}{a\partial \mu}[F_v + P_v] - \nabla^2\left(\frac{u^2+v^2}{2(1-\mu^2)} + \varphi + RT\ln P_s\right), \tag{2}$$

$$\frac{\partial T'}{\partial t} = -\frac{1}{a(1-\mu^2)}\frac{\partial}{\partial \lambda}[U \cdot T'] - \frac{\partial}{a\partial \mu}[V \cdot T'] + D \cdot T' - \dot{\sigma}\frac{\partial T}{\partial \sigma} + k\frac{T\omega}{P} + P_T, \tag{3}$$

$$\frac{\partial q}{\partial t} = -\frac{1}{a(1-\mu^2)}\frac{\partial}{\partial \lambda}[U \cdot q] - \frac{\partial}{a\partial \mu}[V \cdot q] + D \cdot q - \dot{\sigma}\frac{\partial q}{\partial \sigma} + P_q, \tag{4}$$

$$\frac{\partial \ln P_s}{\partial t} = -\vec{V} \cdot \nabla(\ln P_s) - D - \frac{\partial \dot{\sigma}}{\partial \sigma}, \tag{5}$$

$$\frac{\partial \varphi}{\partial \ln \sigma} = -RT. \tag{6}$$

$$\frac{\omega}{P} = \vec{V} \cdot \nabla \ln P_s - \frac{d\ln\sigma}{d\sigma}\int_0^\sigma (D + \vec{V} \cdot \nabla \ln P_s)d\sigma$$

$$\dot{\sigma} = \sigma\int_0^1 (D + \vec{V} \cdot \nabla \ln P_s)d\sigma - \int_0^\sigma (D + \vec{V} \cdot \nabla \ln P_s)d\sigma$$

where

$$\vec{V} \cdot \nabla \ln P_s = \frac{1}{a(1-\mu^2)}\left[U\frac{\partial \ln P_s}{\partial \lambda} + (1-\mu^2)V\frac{\partial \ln P_s}{\partial \mu}\right],$$

$$\zeta = f + \frac{1}{a(1-\mu^2)}\left[\frac{\partial V}{\partial \lambda} - (1-\mu^2)\frac{\partial U}{\partial \mu}\right], \quad f = 2\Omega\sin\varphi,$$

$$D = \frac{1}{a(1-\mu^2)}\left[\frac{\partial U}{\partial \lambda} + (1-\mu^2)\frac{\partial V}{\partial \mu}\right],$$

$$F_u = V \cdot \zeta - \dot{\sigma}\frac{\partial U}{\partial \sigma} - RT'\frac{\partial \ln P_s}{a\partial \lambda},$$

$$F_v = -U \cdot \zeta - \dot{\sigma}\frac{\partial V}{\partial \sigma} - RT'(1-\mu^2)\frac{\partial \ln P_s}{a\partial \mu},$$

$$T' = T - T_0(\sigma), \qquad T_0(\sigma) = \overline{T}_0 = 273.15,$$

$$\nabla^2 = \frac{1}{a^2(1-\mu^2)}\frac{\partial^2}{\partial \lambda^2} + \frac{\partial}{a^2 \partial \mu}\left[(1-\mu^2)\frac{\partial}{\partial \mu}\right],$$

$$U = u\cos\varphi, \quad V = v\cos\varphi, \quad \mu = \sin\varphi.$$

The variables ζ, D, T, q, $\ln P_s$ and φ_s are expanded with spherical harmonics under the triangular truncation:

$$x(\lambda,\mu,\sigma,t) = \sum_{m=-M}^{M}\sum_{n=|m|}^{M} x_{mn}(\sigma,t)P_n^m(\mu)e^{im\lambda}$$

M is the maximum wave number, $M=21$.

(ii) The integrating schemes

The semi-implicit method is adopted and the time step $\Delta t = 45$ minutes. Implicit diffusion term is added to modify the adiabatic results. A process of smoothing the spectral coefficients is carried on each 8 steps (i.e., 6 hours). Wu's (1984) method is adopted here:

$$x_n^{ms} = x_n^m e^{-n(n+1)R}$$

where $R = 5.0 \times 10^{-5}$. As for the long time integration, the restore term is added to balance the dissipation:

$$\frac{x^{t+\Delta t} - x^{t-\Delta t}}{2\Delta t} = \left(\frac{\partial x}{\partial t}\right)_{\text{adiabatic}} - k\nabla^4 x^{t+\Delta t} + k\nabla^4 x^0$$

(iii) The initial data

1958–1973 year–averaged zonal mean climatic data in winter is used as initial fields. $\bar{U}$, $\bar{\varphi}$, $\bar{T}$ are the zonal–mean zonal wind, potential height and temperature fields. Let the meridional wind field v to be zero at the beginning. The moist process is omitted by setting $\bar{q} = 0$. The initial fields are shown in Fig. 1 (a,b,c).

(iv) The schemes of topography

Based on the $1^\circ \times 1^\circ$ orography data (after the U.S. data), several schemes are obtained:

(1) Averaged topography scheme: It is obtained by the average of the orography data near each Gauss–grid point (hereafter referred to as AVE).

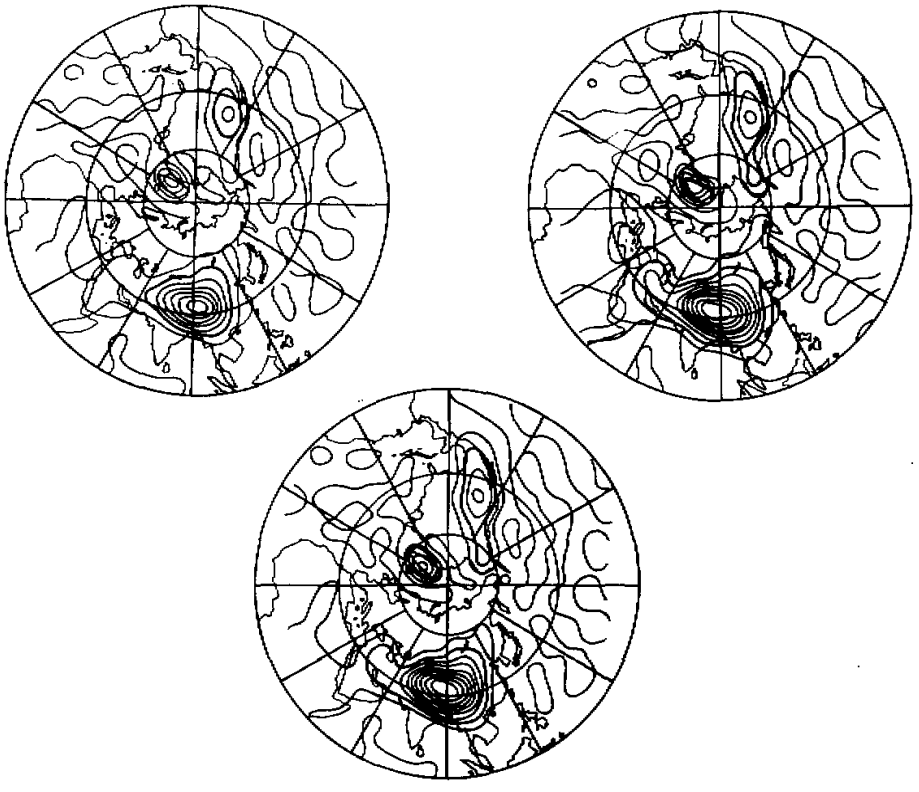

Fig.1. Model topography: (a) the AVE; (b) the ENV; (c) the MEV. unit: meter.

(2) Envelope topography scheme: First the standard deviation of sub–grid orography data is obtained:

$$\sigma_i = \frac{1}{N}\sqrt{\sum_{j=1}^{N}(Z_j - \bar{Z})^2}$$

where j is taken over all the grid points. The envelope topography is obtained by:

$$h_i = \bar{h}_i + 2 \cdot \sigma_i$$

(hereafter referred to as ENV).

After nine-point smooth and spectral truncation, the two topographies are shown in Fig. 1 (a,b). For the former, the maximum altitude is 3600 m situated at (90°E, 35°N) for the TP and 1900m for the RM. For the latter, the maximum altitude is 4600m for the TP and 2200m for the RM. For the ENV, the 1000m-profile agrees well with the reality at the RM when horizontally expanded severely at the TP.

(3) Modified envelope topography scheme: As mentioned above, although the maximum altitude of the TP is increased about 1000m by the ENV, the horizontal expansion is severe. In order to keep the height and slope of the TP as well as to decrease the horizontal expansion, a new topography scheme is devised based on the following procedure:

$$h_i = \bar{h}_i + 2\sigma_i \qquad (\bar{h}_i \geq 1000m)$$
$$h_i = \bar{h}_i \qquad (\bar{h}_i < 1000m)$$

except the region of the North America where the envelope scheme is adopted. The new scheme is hereafter referred to as MEV. As similarly smoothed and truncated as the above two, the new topography is shown in Fig. 1(c). The maximum altitude at TP is still 4600m, but the horizontal expansion has been greatly reduced and approaches the reality. The slope of the main area of the TP is also increased.

III. THE MECHANICAL IMPACT OF THE THREE MODEL TOPOGRAPHIES

Based on the above cited initial data, 10-day integrations are carried on the three topographies respectively.

When the concept of the envelope topography was first mentioned, Wallace et al. (1983) carried out 50-day integrations on the AVE and the ENV for the real-time data on January 21, 1979 with the ECMWF operational model. The last 30-day results were averaged. By comparison with the real data, they found that: (i) the 500hPa simulation with ENV was better, the intensities of both the ridge at Bering Strait and the trough at Alaska Bay were enhanced. But the location of the trough on Europe shifted west; (ii) for 1000 hPa height field, compared with the reality, obvious improvements was at the RM, a weak sea-level ridge appeared at east-side of the RM with ENV whereas strong westerly was simulated acrossing the North America continent with AVE. But in Asia, the coverage and the intensity of the high pressure system were too large and too strong.

In order to make comparison with their results, the 500 hPa height field, the sea-level pressure field and the local zonal-mean wind field are analysed respectively.

(i) The 500 hPa field

Figures 2-3 show the 8th-day 500 hPa height profile on the experiments. The three trough-activity areas are the east coast of Asia, the east of North America continent and Europe, suggesting that some weather patterns usually appearing in the Northern Hemisphere during winter seasons can be roughly simulated by taking only the dynamical effect of topography into account in such an adiabatic model, showing an important role of the dynamic effect of the topography in forcing the Northern Hemisphere circulation in winter.

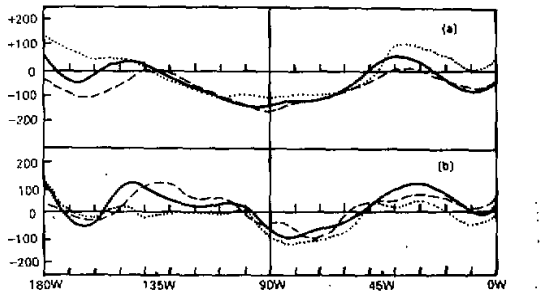

Fig.2. The 8th day 500 hPa height profile for Western Hemisphere. ——AVE, —ENV, ·····MEV. (a) 60°N, (b) 45°N.

The main difference between the ENV and the AVE experiments is that both the ridge at Bering Strait and the trough at Alaska Bay are intensified. The ridge on the Atlantic Ocean is also stronger. It can be clearly seen that the ENV scheme increases the disturbances. It is similar to the results obtained by Wallace et al.

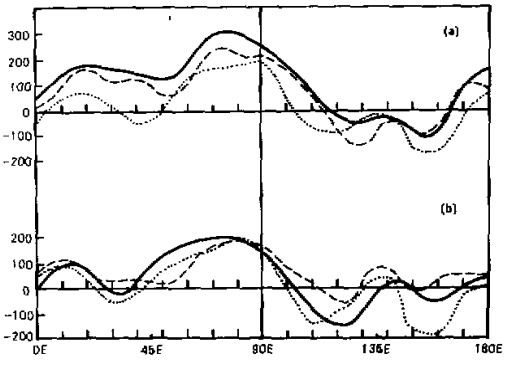

Fig.3. As in Fig. 2 except for Eastern Hemisphere. (a) 40°N, (b) 30°N.

In East Asia, the ridge at 70°E is stronger on the ENV than in the AVE and large differences appear for both the troughs at the up– and down–stream of the ridge at 30°N and 40°N. At 30°N, both the troughs are stronger on the ENV. The situation is just the opposite at 40°N. It can be shown that the increase of the maximum altitude and the expansion of the coverage of TP have very different effects on the perturbations along the north– and south–edge of the TP.

The MEV experiment has shown large difference with ENV experiment. At 30°N, the trough at 150°E is intensified greatly. Another trough appears at its upstream (110°E). At 40°N, the ridge between the two troughs downstream is enhanced. It can be seen from the analysis that the increase of the slope of the TP is favorable for the maintenance of the perturbations at the downstream of the TP. By the same time, anticyclonic vorticity at the high latitudes and cyclonic vorticity at the low latitudes are enhanced.

As for the RM, although the topography schemes have no differences between ENV and

the MEV, the ridge at Bering Strait is intensified while the trough at the Alaska Bay is weakened on the MEV experiment. It can be seen from that the weather patterns for the North America are not only determined by the orography of the RM but also have close relationship with the large-scale orography in Asia.

(ii) The sea-level pressure field

Figure 4(a) shows the 8th-day results on the AVE. At East Asia, the high pressure is centred at (85°E, 36°N) with an intensity of 1036 hPa. There are two low-pressure systems in the area of Okhotsk Sea and Aleutian with an intensity of 986 hPa and 994 hPa respectively. The intensity of the Pacific subtropical high is overestimated as 1026 hPa. The Atlantic subtropical high is also overestimated as 1030 hPa while the intensity of the low pressure system in the north is 986 hPa.

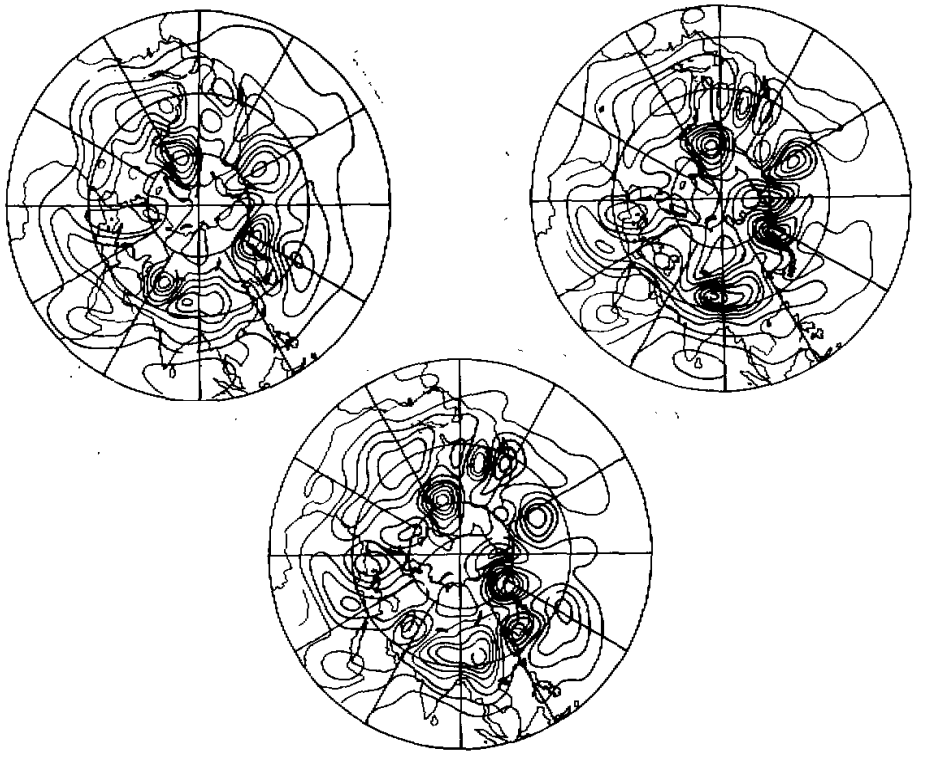

Fig.4. The 8th-day sea surface pressure fields: (a) the AVE; (b) the ENV; (c) the MEV.

The corresponding results on the ENV are shown in Fig. 4(b). The high pressure system in the Asia continent is intensified enormously and reaches 1053 hPa centred at (85°E, 36°N) accompanied by the extending of the coverage of the system. The intensity of the western Pacific Ocean subtropical high is reasonably weakened. The Aleutian low in the upstream of the RM and the Iceland low in the downstream are also intensified to 989 hPa and 980 hPa, respectively. The different effects between the enveloped TP and the enveloped RM are clearly

seen. While the high pressure system is intensified by the enveloped TP, the low pressure systems are enhanced by the enveloped RM.

Figure 4(c) shows the corresponding results on the MEV. The most significant change appears as the eastward movement of the Asia high pressure system centred at (100°E, 35°N) with an intensity of 1042 hPa, more reasonable than the results on the ENV. Comparing with the results obtained by Wallace et al., the MEV topography scheme has significant improvement effects on the simulation of the high pressure system in Asia.

IV. THE AIRFLOW OVER AND AROUND THE OROGRAPHY

The orography has two different dynamical impacts on the currents: (1) to split the currents; (2) to make them flow over the obstacles. The impacts have different effects on different kinds of fluids. For a given fluid, the impacts depend on the features of the orography as well as the state of the currents. We will discuss the different impacts of the three topography schemes from this point of view.

A lot of studies have demonstrated the importance of the altitude of the obstacle in determining the forcing effect on the atmosphere. The dynamic forcing effect of the orography can be expressed at the lower boundary:

$$W_s = U_s \frac{\partial Z_s}{\partial x} + V_s \frac{\partial Z_s}{\partial y}$$

which has included the two effects automatically. Under the linearized process taken by some theoretical works:

$$W_s^{(1)} = \overline{U}_s \frac{\partial z_s}{\partial x}$$

where only the climbing current is included. Wu's (1984) study has indicated that as the altitude of the orography h is between 0–1 km, the linear climbing effect is dominant; as h is between 1–2 km, both the linear–climbing effect and the non–linear split effect are important; when $h>2$ km, the non–linear effect becomes more significant and could not be omitted.

There is no such a theoretical model which can include both the climbing and splitting effects. Although these effects can be included in numerical models, another difficulty is how to distinguish them. In this aspect, we use Qian et al. (1978)'s decomposition method, i.e., to divide the surface wind vector $\vec{V}_s$ into two parts: $\vec{V}_r$ and $\vec{V}_p$ satisfied:

$$\vec{V}_r \cdot \nabla\varphi_s = 0, \quad \vec{V}_r \times \nabla\varphi_s = \vec{V}_s \times \nabla\varphi_s;$$

and

$$\vec{V}_p \times \nabla\varphi_s = 0, \quad \vec{V}_p \cdot \nabla\varphi_s = \vec{V}_s \times \nabla\varphi_s.$$

It is suggested that the split part $\vec{V}_r$ is always at a right angle with the orography slope vector $\nabla\varphi_s$ while the climbing part $\vec{V}_p$ is in the same direction with $\nabla\varphi_s$. We choose the method on the low–level wind vector for the each–day integration and discuss the effects of different topography schemes.

Figure 5(a) shows the 3rd–day splitting component of the low–level wind field on the AVE experiment. There are southward winds at the upstream of the TP and strong northward winds at the downstream, approximately 10 m / s. It can be seen that due to the TP, strong disturbances are generated on the originally uniform zonal flow. Fig. 5(b) shows the

climbing–up component. Compared with Fig. 5(a) the significant difference appears in the region of the TP, of which the altitude is higher than 1 km. The zonal wind speed decreases enormously and the meridional component shows just the opposite pattern to that of Fig. 5(a) —the northward winds in the upstream and the southward winds in the downstream. It is consistent with the analytical theory of the currents climbing up the mountains under the conservation law of the potential vorticity. This also demonstrates the fact that the split component is dominant around the TP in winter season. For the RM, the magnitude of splitting component is comparable to the climbing up component.

As to the ENV experiment, shown in Fig. 6(a,b), the envelope topography makes the northward winds in the dowstream of the TP increase with the maximum speed of 13 m / s. In the RM, the maximum wind speed is 24 m / s. The increase is due to the increase of the climbing–up component. It is also shown the opposite effect of the ENV at the TP and at the RM. While the envelope topography intensifies the split component of the TP, it intensifies the forcing of the climbing–up currents at the RM.

As to the MEV experiment, although the basic pattern is nearly the same as that in the Fig.6, further analysis on the kinetic change can still show the effect of the modified envelope topography. Figure 7 shows a daily–change of the ratio of the kinetic energy of the climbing–up component to the total kinetic energy in the region where the altitude is higher than 1000 m under the three topography schemes. Fig.7(a) is for the TP case. In the AVE experiment, the ratio is about 50%–60%. The ratio drops below 50% in the ENV experiment which is the approvement of the analysis given above. In the MEV experiment, the ratio is even smaller, about 45%. The dominance of the split effect of the TP is most significantly shown in the MEV experiment.

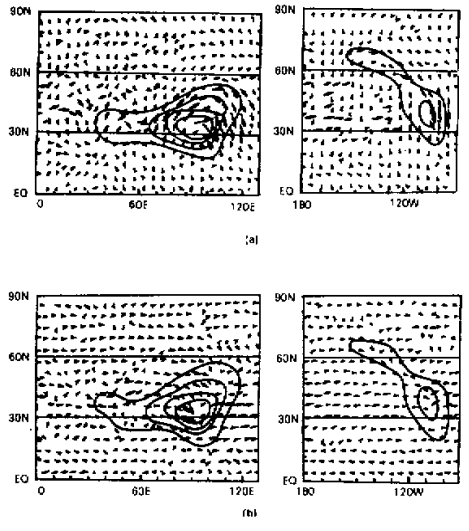

Fig.5. The 3rd day 700 hPa wind fields for AVE. (a) Air flow component around the mountains, (b) the component over the mountains.

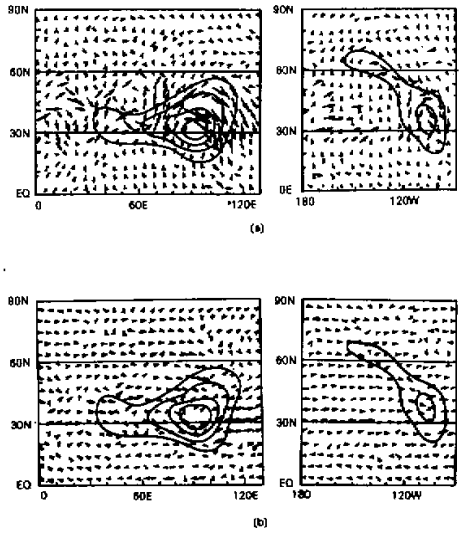

Fig.6. As in Fig. 5 except for ENV.

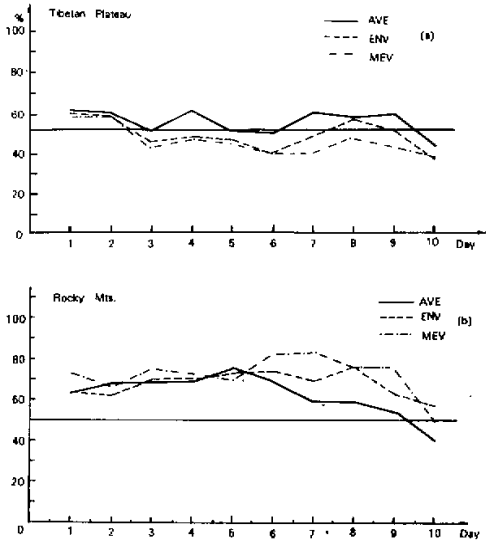

Fig.7. The daily change of the ratio of kinetic energy of the climbing-up component to the total kinetic energy (a) for the Tibetan Plateau (b) for the Rocky Mountains.

In the RM, the situation is just the opposite. In the AVE experiment, the ratio is about 60%–70%, obviously higher than the case of the TP. Only in the later period of the integration (7–10 day), the ratio drops below 60%. In the ENV experiment, although no more change appears in the early period of integration (compared with the case of the AVE), the ratio does not drop as much as in the case of the AVE, except at the 10th-day when the ratio is

below 60%. In the MEV experiment, although the topography is the same as that in the ENV, the ratio shows large changes in the later period of the integration, generally above 70% with the maximum value at 80%. It shows that the climbing–up component is not only determined by the feature of the topography but also by the current patterns. It is just the adoption of the modified topography scheme in Asia that causes the significant changes in the RM at the later period of the integration (Fig. 7(b)).

Based on the above analysis, the different topography schemes cause the different mechanical effects on the currents, which leads to the change of the ratio of the climbing–up part to the split part. The further change of the effects of the different physical processes finally results in the different simulations.

V. THE CONCLUSIONS

From the preceding analysis, the following conclusions are obtained:

(1) In the Northern Hemisphere, the mechanical effects of the large–scale orography play an important role in the circulation of winter season. The common circulation patterns can be obtained by the use of the adiabatic two–layer spectral model which has incorporated the real orography.

(2) Different topography schemes can result in significant different air motions. By the over extension of the 1000 m coverage of the TP, the simulation of the envelope orography is severely influenced.

(3) After the modification to the envelope topography by decreasing the horizontal expansion while keeping the maximum altitude, the simulation is improved significantly. And the center and the intensity of the simulated high pressure system in Asia are more reasonable.

(4) Through the control experiment on the split and climbing–up components, the distinctively different mechanical effects of the TP and the RM are shown clearly. For the former, the split currents are dominative while for the latter, the climbing–up currents dominate. The improved simulations by use of the ENV and the MEV results from the changes of the ratio of the two components.

As to the lower resolution used by the model in both the horizontal and vertical directions, further experiments should be carried on the high resolution models with the diabatic physical processes.

REFERENCES

Chen Jiabin, Ji Liren and Wu Wanli (1987), Design and test of an improved scheme for global spectral model with reduced truncation error, *Advances in Atmos. Sci.* **4**: 156–168.

Dell'Osso, Radinovic (1984), A case study of cyclone development in the lee of the Alps on 18 March, 1982, *Beitr. Phys. Atmos.*, **57**: 369–379.

Egger, J. (1970), On the simulation of sub–grid orographic effects in the numerical forecasting, *JAS*, **27**: 896–902.

Egger, J. (1972), Incorporation of the steep mountains into forecasting model, *Tellus*, **24**: 324–335.

Eliassen, A. and Palm, E. (1961), On the transfer of energy in stationary mountain waves, *Geophys. Publ.*, **22(3)**: 1–23.

Jarrand, M. (1985), Impact of an envelope orography in the ECMWF model, ECMWF Seminar 1985, **2**: 199–249.

Mesinger, F. and Strikler, R.F. (1982), Effect of mountains on Genoa cyclogenesis, *J. Meteor. Soc. Japan*, **60**: 326–338.

Palmer, T.N. et al. (1987), Alleviation of a systematic westerly bias in general circulation and numerical weather prediction models through an orographic gravity wave drag parametrization, *Quart. J. R., Meteor. Soc.*, **113**: 706–707.

Qian Yongfu et al. (1978), A primitive equation numerical prediction model including the influence of the large-scale orography, *Scientia Atmospherica. Sinica*, **2**: 91–102.

Shutts, G.J. (1985), Parametrization of sub-grid scale gravity wave mountain transfer and its influences in forecast / climate models, ECMWF Seminar 1985, **2**: 167–198.

Tsai, M–C, and Krishnamurti, T.N. (1986), Numerical prediction of a surge vortex during winter monsoon, *J. Meteor. Soc.*, Japan, **64**: 505–517.

Wallace et al. (1983), Reduction of systematic forecast errors in the ECMWF model through the introduction of an envelope orography, *Quart. J. R, Meteor. Soc.*, **109**: 683–717.

Wu, G.X. (1984), The nonlinear response of the atmosphere to large-scale mechanical and thermal forcing, *JAS*, **41**: 2456–2476.

Wu, G.X., and Chen, S. J. (1984), The effect of mechanical forcing on the formation of a mesoscale vortex, ECMWF Technical Report No. 45.